7 **Mitoma H**, Song SY, Ishida K, *et al*. Presynaptic impairment of cerebellar inhibitory synapses by an autoantibody to glutamate decarboxylase. *J Neurol Sci* 2000;**175**:40–4.
8 **Saito Y**, Suzuki K, Nanba E, *et al*. Niemann-Pick type C disease: accelerated neurofibrillary tangle formation and amyloid beta deposition associated with ApoE ε4 homozygosity. *Ann Neurol* 2002;**52**:351–5.
9 **Caesmans M**, Smitt PA, Linden DJ, *et al*. Mechanisms underlying cerebellar motor deficits due to mGluR1-autoantibodies. *Ann Neurol* 2003;**53**:325–36.
10 **Verschuuren J**, Chuang L, Rosenblum MK, *et al*. Inflammatory infiltrates and complete absence of Purkinje cells in anti-Yo-associated paraneoplastic cerebellar degeneration. *Acta Neuropathol (Berl)* 1996;**91**:519–25.
11 **Nakanishi K**, Kobayashi T, Miyashita H, *et al*. Relationships among residual beta cells, exocrine pancreas, and islet cell antibodies in insulin-dependent diabetes mellitus. *Metabolism* 1993;**42**:196–203.
12 **Gatti RA**, Vinters HV. Cerebellar pathology in ataxia telangiectasia: the significance of basket cells. *Kroc Found Ser* 1985;**19**:225–32.
13 **Mitoma H**, Ishida K, Shizuka-Ikeda M, *et al*. Dual impairment of GABAA- and GABAB-receptor-mediated synaptic responses by autoantibodies to glutamic acid decarboxylase. *J Neurol Sci* 2003;**208**:51–6.
14 **Meinck HM**, Ricker K, Hulser PJ, *et al*. Stiff man syndrome: clinical and laboratory findings in eight patients. *J Neurol* 1994;**241**:157–66.
15 **Warren JD**, Scott G, Blumbergs PC, *et al*. Pathological evidence of encephalomyelitis in the stiff man syndrome with anti-GAD antibodies. *J Clin Neurosci* 2002;**9**:328–9.
16 **Warich-Kirches M**, Von Bossanyi P, Treuheit T, *et al*. Stiff-man syndrome: possible autoimmune etiology targeted against GABA-ergic cells. *Clin Neuropathol* 1997;**16**:214–19.

ELSEVIER

Journal of the Neurological Sciences 254 (2007) 44–48

Journal of the Neurological Sciences

www.elsevier.com/locate/jns

A Japanese family with early-onset ataxia with motor and sensory neuropathy

Shunsuke Kobayashi [a,b,*], Hiroshi Takuma [a,c], Shigeo Murayama [a,d], Masaki Sakurai [a,e], Ichiro Kanazawa [a,f]

[a] Department of Neurology, Division of Neuroscience, Graduate School of Medicine, University of Tokyo, Tokyo, Japan
[b] Department of Physiology, Development, and Neuroscience, University of Cambridge, United Kingdom
[c] Department of Molecular Neurobiology, Max-Planck Institute for Medical Research, Heidelberg, Germany
[d] Department of Neuropathology, Tokyo Metropolitan Institute of Gerontology, Tokyo, Japan
[e] Department of Physiology, Teikyo University School of Medicine, Tokyo, Japan
[f] National Center of Neurology and Psychiatry, Tokyo, Japan

Received 16 July 2006; received in revised form 8 December 2006; accepted 18 December 2006
Available online 29 January 2007

Abstract

We report the case of a Japanese family with hereditary ataxia with peripheral neuropathy. Three affected siblings from this family exhibited very similar clinical features: teenage-onset, slowly progressive ataxia, followed by distal weakness, which developed after the age of 30 years. Magnetic resonance imaging studies showed marked atrophy in the cerebellar hemisphere and vermis, and a sural nerve biopsy revealed a marked reduction in the number of both myelinated and unmyelinated fibers. All patients exhibited hyperglutamatemia, but serum levels of albumin and lipid were normal. The clinicopathological and biochemical features of these cases suggest that they form a distinct entity of autosomal recessive hereditary ataxia with peripheral neuropathy.

Keywords: Cerebellar atrophy; Peripheral neuropathy; Autosomal recessive inheritance; Hyperglutamatemia

1. Introduction

Hereditary ataxia is sometimes associated with peripheral neuropathy, and it appears to comprise a heterogeneous group of diseases. The most common of these diseases among the Caucasian population is Friedreich's ataxia (FA), which is caused by mutation of the *frataxin* gene [1]. However, no patients with FA have been reported in the Japanese population. Early-onset ataxia with ocular motor apraxia and hypoalbuminemia (EAOH), which is caused by a mutation of the *aprataxin* gene, forms a homogeneous group within the Japanese population who suffer from hereditary ataxia associated with peripheral neuropathy [2,3]. Various types of hereditary ataxia with peripheral neuropathy have been reported [4,5], but their clinical entity remains unclear. Here we report the familial cases of patients with early-onset ataxia with severe motor and sensory neuropathy and hyperglutamatemia.

2. Patients and clinical evaluation

Three patients (two males and one female), who are siblings (Fig. 1), were diagnosed with ataxia and motor sensory neuropathy, based on clinical, neuroradiological, and neuropathological findings. Their parents were cousins who died in their 90s and had no signs of the disease. Patients IV-3 and IV-6 were admitted to Tokyo University Hospital when they were 63 and 52 years old, respectively. Patient IV-4 was examined by one of the authors at a nursing

* Corresponding author. University of Cambridge, Department of Physiology, Development and Neuroscience, Downing Street, Cambridge CB2 3DY, United Kingdom. Tel.: +44 1223 339544; fax: +44 1223 333786.
E-mail address: skoba-tky@umin.ac.jp (S. Kobayashi).

0022-510X/$ - see front matter © 2007 Elsevier B.V. All rights reserved.
doi:10.1016/j.jns.2006.12.014

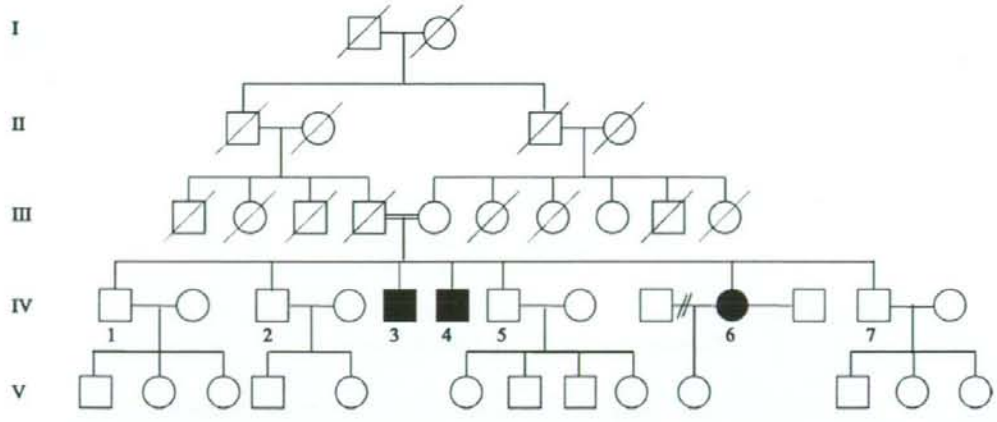

Fig. 1. Pedigree of the family. Squares and circles indicate males and females, respectively. Filled symbols represent affected individuals.

house when he was 61 years old. Three siblings of these patients (IV-1, IV-2, and IV-7) were also examined and no positive neurological signs were detected.

The clinical histories of the three affected siblings resemble each other closely. The first symptom of the disease, gait instability, was noted at age 15, 17, and 18 years in patients IV-3, IV-4, and IV-6, respectively. In all patients, limb and truncal ataxia progressed mainly in their 20s, and muscular weakness of the upper and lower distal extremities progressed mainly in their 30s and 40s. These patients were confined to a wheelchair at the age of 47 years (patient IV-3), 44 years (patient IV-4), and 39 years (patient IV-6). Patients IV-3 and IV-4 were both diagnosed as mildly diabetic at the age of 52 years. At age 55 years, patient IV-3 was diagnosed with reflux esophagitis, and patient IV-4 developed cholelithiasis at the age of 58 years.

On examination, two of the patients showed a normal range of intelligence (patient IV-3: WAIS-R IQ 84, VIQ 95, PIQ 72; patient IV-4: full score in Mini-Mental Scale Examination). Patient IV-6 showed mild cognitive impairment (WAIS-R IQ 65, VIQ 84, PIQ 50, Raven's progressive color matrices 22/37). In all patients, external eye movements were full, but smooth pursuit was abnormally saccadic. Ocular motor apraxia was not present. Lateral gaze nystagmus was observed in all patients and rebound nystagmus was remarkable in patient IV-6. None of the patients had any other ophthalmologic abnormalities, including retinitis pigmentosa. Speech was slurred and ataxic in all three patients, and their distal extremities exhibited wasting and weakness, especially the lower extremities. The musculature in the proximal extremities was well preserved. All patients had sensory loss of all modalities in a "glove and stocking" distribution. Deep tendon reflexes were all absent. None of the patients exhibited pathological reflexes. Although evaluation of coordination was difficult due to severe distal limb weakness, all of the patients showed large oscillatory movement on the finger-to-nose test, suggesting the presence of limb ataxia. Patient IV-6 had mild scoliosis. None of the patients had cardiopulmonary abnormalities.

3. Laboratory study

Blood cell counts were normal in all three patients. Routine blood chemistry was normal, with the exception of high glycosylated hemoglobin A1c in patient IV-4 (7.7%). Serum alpha-fetoprotein, lactate, pyruvate, cholestanol, plasma vitamin E, very long-chain fatty acid, ceruloplasmin, beta-lipoprotein, leukocyte liposome enzymes, CSF cell count and protein level were within the normal ranges in all three patients. Plasma transferrin isofocusing showed normal property, excluding the diagnosis of congenital disorders of glycosylation. Plasma glutamate levels were higher than normal in all three patients (Table 1). All examined unaffected siblings (IV-1, IV-2, and IV-7) showed normal levels of plasma glutamate (<63 nmol/ml). The results of genetic screening for SCA1, SCA2, MJD, DRPLA, PMP22, and P0, carried out for patients IV-3 and IV-6, were all negative.

4. Neuroimaging study

Brain MRI showed a marked atrophy of the cerebellar hemisphere and vermis in all three patients. There was no clear atrophy in the cerebral cortex and the brainstem (Fig. 2A–C).

5. Electrodiagnostic study

Electrodiagnostic studies were performed in patients IV-3 and IV-6. Motor NCVs were reduced in both patients.

Table 1
Summary of biochemical data

	Patients			Normal range
	IV-3	IV-4	IV-6	
Serum total protein (g/dl)	6.2	6.8	6.9	6.2–8.2
Serum albumin (g/dl)	3.4	3.8	3.6	3.4–5.8
Serum total cholesterol (mg/dl)	136	150	162	130–220
Serum triglyceride (mg/dl)	76	80	92	50–150
Serum β-lipoprotein (mg/dl)	252	271	315	190–500
Plasma glutamate (nmol/ml)	140	158.5	130	12–63

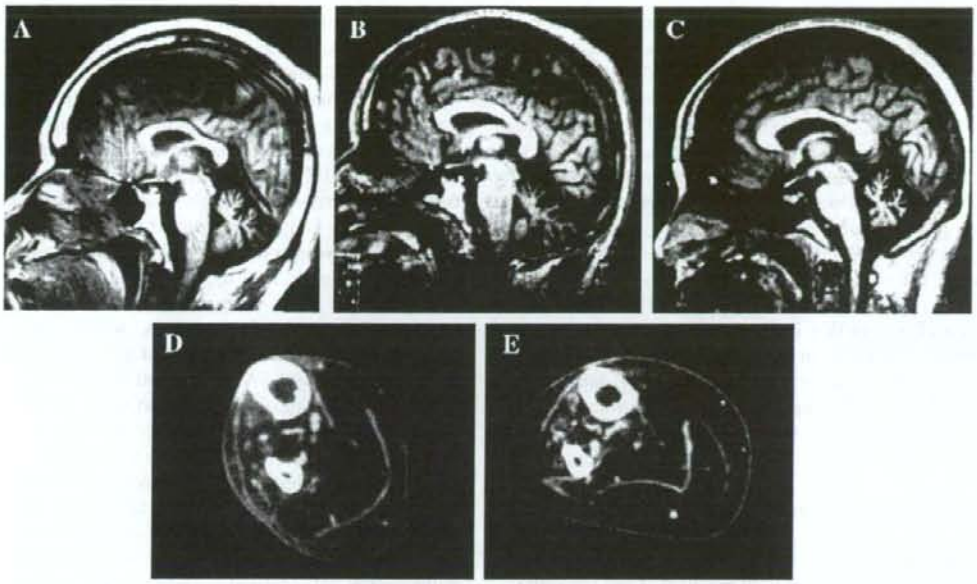

Fig. 2. Brain magnetic resonance imaging (MRI) and muscle computed tomography (CT) images. A–C: Sagittal planes of T1-weighted MRI images in patients IV-3 (A), IV-4 (B), and IV-6 (C). All images show marked atrophy of the cerebellar vermis. D, E: CT scans of calf muscles in patients IV-3 (D) and IV-6 (E). The low-density appearance of the muscles indicates fatty degeneration.

Compound muscle action potentials (CMAP) were markedly low [NCV (m/s)/CMAP (mV) patient IV-3: median nerve 25/0.046, ulnar nerve 26/0.013, tibial nerve — not detected, peroneal nerve — not detected; patient IV-6: median nerve 41/1.77, ulnar nerve 44/1.42, tibial nerve — not detected, peroneal nerve 53/0.32]. Sensory nerve action potentials were not detected in either patient IV-3 or IV-6 at any of the tested nerves. Needle electromyography demonstrated

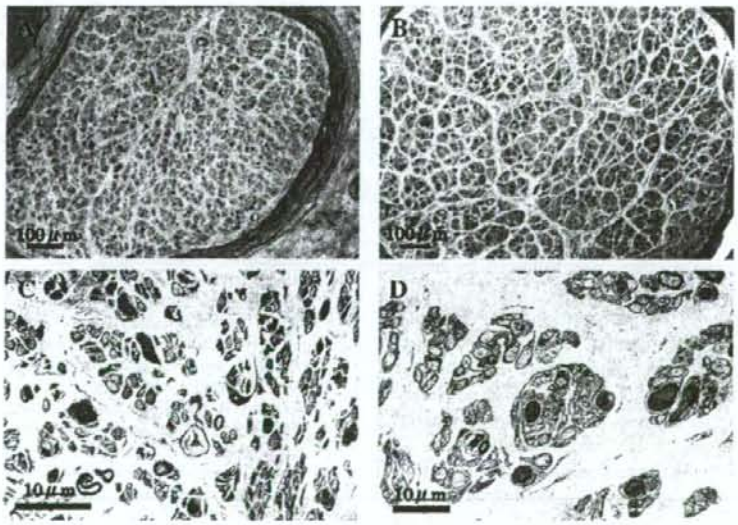

Fig. 3. Sural nerve biopsy specimens. A, B: Light microscopy of transverse semithin sections of the distal sural nerve (A: patient IV-3, magnification ×1200, toluidine blue stain; B: patient IV-6, magnification ×1000, toluidine blue stain). C, D: Electron micrographs of sural nerves (C: patient IV-3, magnification × 25,000; D: patient IV-6, magnification ×33,000).

spontaneous fibrillation potentials in the hand muscles of both of these patients. On volitional muscle contraction, discharges had a high amplitude and long duration in all examined muscles except the tibialis anterior muscle, where no discharge was observed. The quantity of discharges was markedly reduced, especially in the leg muscles. In summary, needle electromyography examination indicated chronic neurogenic change that was more severe in the distal than the proximal muscles.

6. Muscle CT

Patients IV-3 and IV-6 both exhibited similar findings on the muscle CT. Muscles in the lower extremities showed low density, indicating fat replacement (Fig. 2D and E). In contrast, the truncal, paraspinal, and limb-girdle muscles were well preserved. The forearm muscles were atrophic in patient IV-6.

7. Neuropathological study

Examination of the sural nerves revealed a marked reduction in the numbers of both myelinated and unmyelinated fibers in patients IV-3 and IV-6 (Fig. 3). Proof of demyelination/remyelination was not found in either case. Fiber density was 825/mm^2 in patient IV-3 (normal range: 7500–10,000/mm^2).

8. Discussion

The clinical picture of the cases reported here is a combination of spinocerebellar degeneration (SCD) and hereditary motor sensory neuropathy (HMSN). Healthy consanguineous parents and three affected siblings in this family suggest autosomal recessive inheritance. The involvement of the central nervous system appears to be limited to the cerebellum, except for mild cognitive impairment in one patient. Conduction studies and morphologic studies indicated that peripheral nerve involvement in our patients was axonal neuropathy, which was much more severe than that reported for some autosomal dominant SCDs [6–8]. In all three patients, cerebellar ataxia, which developed in their teenage years, was followed by motor sensory neuropathy in their 30s or 40s.

Differential diagnoses of Refsum disease, Bassen–Kornzweig disease, metachromatic leukodystrophy, and congenital disorders of glycosylation were excluded by laboratory tests. Ataxia-oculomotor apraxia 1 is not likely because of its earlier age at onset and oculomotor apraxia. Ataxia-oculomotor apraxia 2 can be excluded because of normal alpha-fetoprotein level in our patients. Mitochondrial disorders are not likely because of normal serum lactate and pyruvate levels in our patients. Absence of spasticity and retinal involvement makes the diagnosis of autosomal recessive spastic ataxia of Charlevoix–Saguenay unlikely. Cerebrotendinous xanthomatosis is excluded because of the normal level of serum cholestanol and lack of xanthoma formation. Fukuhara et al. reported patients with HMSN associated with cerebellar atrophy (HMSNCA) who showed hypoalbuminemia and hyperlipidemia [9]. Recently, it was demonstrated that an atypical form of FA in Japan, labeled EAOH, was caused by mutation of the *aprataxin* gene [2]. Diagnoses of HMSNCA [9,10] and EAOH [3] are unlikely because of normal serum albumin and total cholesterol levels in our patients. Tanji et al. reported a Japanese family with progressive cerebellar ataxia, distal amyotrophy of Charcot–Marie–Tooth type and hyperglutamatemia [11], which resembles our cases very much. Present cases together with Tanji's cases appear to form a clinical entity distinct from previously reported diseases of ataxia with peripheral neuropathy including FA, EAOH and HMSNCA.

Hyperglutamatemia was observed in all of our patients and in none of the three unaffected siblings. The results indicate involvement of glutamate in the pathogenesis of the present disorder. Glutamate is the most abundant free amino acid in the central nervous system playing a prominent role in synaptic plasticity, learning and memory. Glutamate is also a potent neuronal excitotoxin, implicated in the pathogenesis of cerebral ischemia, and epilepsy [12]. Experimentally, infusions of high concentrations of glutamate elicit neuronal degeneration by, at least in part, enhanced calcium entry in the cytosol through excessive stimulation of the *N*-methyl-D-aspartate (NMDA) receptors. Hyperglutamatemia has also been reported in some neurodegenerative diseases [12–14]. Partial deficiency of the enzyme glutamate dehydrogenase in fibroblasts, leukocytes, and platelets has been reported to occur in various types of ataxia [13,14], and it does not appear to identify a specific type of ataxic disease [15,16]. Hyperglutamatemia in our patients suggests some form of abnormality of glutamate metabolism, but it is difficult to speculate its role in the pathogenesis of their disease. Future investigation on genetic and biochemical aspects of this disease is important, because it might lead to therapeutic interventions by blocking NMDA- and non-NMDA-receptor mediated neurotoxicity.

References

[1] Campuzano V, Montermini L, Molto MD, Pianese L, Cossee M, Cavalcanti F, et al. Friedreich's ataxia: autosomal recessive disease caused by an intronic GAA triplet repeat expansion. Science 1996;271:1423–7.
[2] Date H, Onodera O, Tanaka H, Iwabuchi K, Uekawa K, Igarashi S, et al. Early-onset ataxia with ocular motor apraxia and hypoalbuminemia is caused by mutations in a new HIT superfamily gene. Nat Genet 2001;29:184–8.
[3] Shimazaki H, Takiyama Y, Sakoe K, Ikeguchi K, Niijima K, Kaneko J, et al. Early-onset ataxia with ocular motor apraxia and hypoalbuminemia: the aprataxin gene mutations. Neurology 2002;59:590–5.
[4] Tachi N, Kozuka N, Ohya K, Chiba S, Sasaki K. Hereditary cerebellar ataxia with peripheral neuropathy and mental retardation. Eur Neurol 2000;43:82–7.
[5] Yamashita I, Sasaki H, Yabe I, Kikuchi S, Chin S, Fukazawa T, et al. Recessively inherited spastic paraplegia associated with ataxia, congenital cataracts, thin corpus callosum and axonal neuropathy. Acta Neurol Scand 2000;102:65–9.

[6] Schols L, Amoiridis G, Buttner T, Przuntek H, Epplen JT, Riess O. Autosomal dominant cerebellar ataxia: phenotypic differences in genetically defined subtypes? Ann Neurol 1997;42:924–32.
[7] van de Warrenburg BP, Notermans NC, Schelhaas HJ, van Alfen N, Sinke RJ, Knoers NV, et al. Peripheral nerve involvement in spinocerebellar ataxias. Arch Neurol 2004;61:257–61.
[8] Klockgether T, Schols L, Abele M, Burk K, Topka H, Andres F, et al. Age related axonal neuropathy in spinocerebellar ataxia type 3/ Machado–Joseph disease (SCA3/MJD). J Neurol Neurosurg Psychiatry 1999;66:222–4.
[9] Fukuhara N, Nakajima T, Sakajiri K, Matsubara N, Fujita M. Hereditary motor and sensory neuropathy associated with cerebellar atrophy (HMSNCA): a new disease. J Neurol Sci 1995;133:140–51.
[10] Sekijima Y, Ohara S, Nakagawa S, Tabata K, Yoshida K, Ishigame H, et al. Hereditary motor and sensory neuropathy associated with cerebellar atrophy (HMSNCA): clinical and neuropathological features of a Japanese family. J Neurol Sci 1998;158:30–7.
[11] Tanji H, Takeda A, Tateyama M, Mochizuki H, Itoyama Y. Progressive cerebellar ataxia and distal amyotrophy of Charcot–Marie–Tooth type with hyperglutamataemia: two sibling case. Clin Neurol 1995:793–7.
[12] Greenamyre JT. The role of glutamate in neurotransmission and in neurologic disease. Arch Neurol 1986;43:1058–63.
[13] Plaitakis A, Berl S, Yahr MD. Abnormal glutamate metabolism in an adult-onset degenerative neurological disorder. Science 1982;216:193–6.
[14] Plaitakis A, Berl S, Yahr MD. Neurological disorders associated with deficiency of glutamate dehydrogenase. Ann Neurol 1984;15:144–53.
[15] Aubby D, Saggu HK, Jenner P, Quinn NP, Harding AE, Marsden CD. Leukocyte glutamate dehydrogenase activity in patients with degenerative neurological disorders. J Neurol Neurosurg Psychiatry 1988;51:893–902.
[16] Duvoisin RC, Nicklas WJ, Ritchie V, Sage J, Chokroverty S. Low leukocyte glutamate dehydrogenase activity does not correlate with a particular type of multiple system atrophy. J Neurol Neurosurg Psychiatry 1988;51:1508–11.

J Neuropathol Exp Neurol

Vol. 66, No. 5
May 2007
pp. 354–362

ORIGINAL ARTICLE

Analysis of the Adrenal Gland Is Useful for Evaluating Pathology of the Peripheral Autonomic Nervous System in Lewy Body Disease

Yuichi Fumimura, MD, Masako Ikemura, MD, Yuko Saito, MD, PhD, Renpei Sengoku, MD, Kazutomi Kanemaru, MD, PhD, Motoji Sawabe, MD, PhD, Tomio Arai, MD, PhD, Genta Ito, MSc, Takeshi Iwatsubo, MD, PhD, Masashi Fukayama, MD, PhD, Hidehiro Mizusawa, MD, PhD, and Shigeo Murayama, MD, PhD

Abstract

Lewy body disease is defined as Lewy body-related neuronal degeneration involving the nigrostriatal system, limbic-neocortical system, and peripheral autonomic nervous system (PANS). We investigated whether the adrenal gland, which is evolutionarily related to sympathetic ganglia and is routinely examined in general autopsy, could be used to assess pathology of the PANS in Lewy body disease. Brains, spinal cords, and adrenal glands from 783 consecutive autopsy cases from a general geriatric hospital were examined immunohistochemically with antiphosphorylated α-synuclein antibodies and routine staining. Parkinson disease (PD) with dementia and dementia with Lewy bodies (DLB) were defined using 1996 Consensus Guidelines for DLB and the secondary Lewy body-related α-synucleinopathy or amygdala variants using previously established criteria. Lewy body-related α-synucleinopathy was found in 207 (26.4%) of 783 cases, with 1 case solely in the adrenal gland. In all 18 PD cases with or without dementia and in 33 of 38 DLB cases, the adrenal gland was involved, but it was spared in all cases of amygdala variants. Our results indicate that the adrenal gland can provide useful information for evaluation of the PANS in Lewy body disease.

Key Words: Alzheimer disease, Amygdala variant, Autonomic failure, Dementia with Lewy bodies, Parkinson disease, Sympathetic ganglion, α-Synucleinopathy.

INTRODUCTION

Lewy body disease was originally defined pathologically as degeneration of the central nervous system associated with Lewy bodies (1, 2) and includes Parkinson disease (PD) and dementia with Lewy bodies (DLB). Subsequently, clinical and pathologic studies indicated that progressive autonomic failure of the Lewy body type presented with Lewy body-related pathology in the peripheral autonomic nervous system, as well as in the central nervous system (3). Clinical and pathologic studies confirmed that DLB always accompanies Lewy body-related pathology in the peripheral autonomic nervous system (4). Thus, it is more practical to use the term "Lewy body disease" to designate disorders involving both the central nervous system and the peripheral autonomic nervous system, which clinically present with various combinations of parkinsonism, cognitive decline, or autonomic failure (5).

Clinical evaluation of the involvement of the peripheral autonomic nervous system in Lewy body disease has been improved by the adoption of [^{123}I]metaiodobenzylguanidine (MIBG) cardiac scintigraphy (6), which shows low uptake of ^{123}I in PD and progressive autonomic failure (7, 8). Histologically, this low uptake corresponds to a decrease in the number of tyrosine hydroxylase-immunoreactive axons (9) associated with α-synucleinopathy in the epicardium of the anterior wall of the left ventricles of the heart (10) seen on postmortem examination. MIBG cardiac scintigraphy reportedly has 100% specificity and sensitivity for the differential diagnosis of DLB and Alzheimer disease (AD) (11). Thus, evaluation of the peripheral autonomic nervous system is now a standard for confirmation of the pathologic diagnosis of Lewy body disease.

From the Department of Neuropathology (YF, MI, YS, RS, SM), Tokyo Metropolitan Institute of Gerontology, Tokyo, Japan; Department of Neurology and Neurological Science (YF, HM), Graduate School, Tokyo Medical and Dental University, Tokyo, Japan; Department of Human Pathology (MI, MF), Graduate School of Medicine, The University of Tokyo, Tokyo, Japan; Department of Pathology (YS, MS, TA), Tokyo Metropolitan Geriatric Hospital, Tokyo, Japan; Department of Neurology (RS), The Jikei University School of Medicine, Tokyo, Japan; Department of Neurology (KK), Tokyo Metropolitan Geriatric Hospital, Tokyo, Japan; Department of Neuropathology and Neuroscience (GI, TI), Graduate School of Pharmaceutical Science, The University of Tokyo, Tokyo, Japan.

Drs. Fumimura and Ikemura contributed equally to this work.

Send correspondence and reprint requests to: Yuko Saito, MD, PhD, Department of Neuropathology, Tokyo Metropolitan Institute of Gerontology, 35-2 Sakaecho, Itabashi-ku, Tokyo 173-0015, Japan; E-mail: yukosa@tmig.or.jp

This work was supported by grants from Aid for Scientific Research on Priority Areas–Advanced Brain Science Project from the Ministry of Education, Culture, Sports, Science and Technology of Japan (SM, YS), Aid for Degenerative Disease from the Ministry of Health, Labor and Welfare (SM), Aid for Long-Term Comprehensive Research on Age-Associated Dementia from the Tokyo Metropolitan Institute of Gerontology (SM), and the Tokyo Metropolitan Geriatric Hospital (YS).

The sympathetic ganglia are the most widely used specimen for the evaluation of the peripheral autonomic nervous system in Lewy body disease (12). However, these ganglia and the epicardium of the anterior wall of the left ventricle of the heart are not a routine site for investigation in general autopsy. In contrast, the adrenal gland is always included in routine autopsy examinations and is a good candidate for examination of the peripheral autonomic nervous system because it is evolutionarily related to sympathetic ganglia and includes autonomic nerves and ganglia in the capsular fatty tissue. Several previous studies indicated that the adrenal gland might be involved in PD (13). However, the exact incidence of adrenal gland involvement in Lewy body disease is not well established.

We recently reported a staging paradigm for Lewy body-related α-synucleinopathy (LBAS) in consecutive autopsy cases roughly representing a general cohort of the elderly (14, 15). Employing the same strategy in the present study, we provide evidence that evaluation of the peripheral autonomic nervous system in Lewy body disease is possible through the examination of archival paraffin blocks of adrenal glands. Our studies also suggest that adrenal involvement may be associated with orthostatic hypotension in Lewy body disease.

MATERIALS AND METHODS

Tissue Source

For the present study, we used 783 consecutive autopsy brains, spinal cords, and adrenal glands obtained from the Tokyo Metropolitan Geriatric Hospital (TMGH). This hospital provides community-based medical service to the aged population 24 hours/day in cooperation with local general practitioners. The number of patients requiring emergency admission to the hospital reaches almost 5,000 per year. The hospital holds 711 beds in its ward and is directly run by the Tokyo Metropolitan Government to promote the health and welfare of an aged population of nearly 1 million residents of the Tokyo metropolitan area. In the present study, 452 of the 783 examined cases overlapped cases used in a previous study (15). The patient ages ranged from 48 to 104 years (80.68 ± 8.8 years, mean ± SD) at the time of death, and the male to female ratio was 455:328. The postmortem interval ranged from 52 minutes to 88 hours (13.16 ± 6:36 hours). Tissue samples were collected after informed consent was obtained from relatives of the deceased according to the Article 18 of the Cadavers Autopsy and Preservation Act in Japan.

Neuropathology

Routine Staining

All brains and spinal cords were examined as described previously (15). Briefly, 6-μm-thick sections of the representative anatomical areas were stained with hematoxylin and eosin using the Klüver-Barrera method and further examined by means of modified methenamine (16) and Gallyas-Braak silver (17) staining to detect senile changes, Congo red staining to detect amyloid deposition, and elastica Masson trichrome staining to detect vascular changes. In addition, the bilateral adrenal glands were fixed in 10% buffered formalin and embedded in paraffin and then 3-μm-thick serial sections were obtained for hematoxylin and eosin staining.

Immunohistochemistry

A Ventana NX20 autoimmunostainer (Ventana, Tucson, AZ) was used (18) with the following antibodies: anti-phosphorylated tau (ptau) (AT8, monoclonal; Innogenetics, Temse, Belgium), anti-β amyloid (11–28, 12B2, monoclonal; IBL, Maebashi, Japan), anti-phosphorylated α-synuclein (psyn#64 [14] and Pser129 polyclonal [19]), anti-α-synuclein (LB509, amino acids 115–122 [20], monoclonal), anti-ubiquitin (polyclonal, Sigma-Aldrich, St. Louis, MO), anti-phosphorylated neurofilament (SMI31, monoclonal; Sternberger Immunochemicals, Bethesda, MA) and anti-tyrosine hydroxylase (anti-TH, monoclonal; Calbiochem-Novabiochem Corporation, Darmstadt, Germany).

TABLE 1. Lewy Body (LB) Stages in the Central Nervous System (14, 15)

Stage	Substantia Nigra and Locus Ceruleus: Loss of Pigmentation	LB				Dementia	Parkinsonism	Diagnosis
		Nigrostriatal	Limbic-Neocortical	Spinal Cord	LB Score			
0	−	−	−	−	0			
0.5	−	+/−	+/−	+/−	0			
I	−	+/−	+/−	+/−	0			Incidental LB disease
II	+	+	+/−	+/−	0–10	−*	−*	Subclinical LB disease
III	+	+	+	+	0–10	−	+	PD
IV	+	+	+	+	3–6	+	+	PDDT
							+/−	DLBT†
V	+	+	+	+	7–10	+	+	PDDN
							+/−	DLBN†

*, No dementia or parkinsonism associated with Lewy body-related α-synucleinopathy.

†, Differential diagnosis of PDD and DLB was based on the "1-year rule" according to the Consensus Guidelines (21).

LB, Lewy body; DLBN, dementia with Lewy bodies, with a Lewy body score corresponding to the value for the neocortical form; DLBT, dementia with Lewy bodies, with a Lewy body score corresponding to the value for the transitional form; PDDN, Parkinson disease with dementia, with a Lewy body score corresponding to the value for the neocortical form; PDDT, Parkinson disease with dementia, with a Lewy body score corresponding to the value for the transitional form.

Lewy Body-Related Pathology

Central Nervous System

The medulla oblongata at the level of the dorsal motor nucleus of the vagus, the upper pons at the level of the locus ceruleus, and the midbrain (including the substantia nigra, the amygdala, and the anterior hippocampus from all cases) were immunohistochemically stained with anti-phosphorylated α-synuclein antibodies. When positive results were obtained in any case, the anterior cingulate gyrus, the entorhinal cortex, the second frontal and temporal gyri, and the supramarginal gyrus were immunohistochemically examined using anti-ubiquitin antibody to provide Lewy body scores (21), and the results were confirmed using anti-α-synuclein and anti-phosphorylated α-synuclein antibodies. The basal nucleus of Meynert (22), CA2-3 of the posterior hippocampus (23), and several (at least upper, middle, and lower) levels of the thoracic spinal cord were also examined with the anti-phosphorylated α-synuclein antibodies. The Lewy body stage (Table 1) was determined for all the cases examined, as reported previously (14, 15). In this study, we added Stage 0.5 as Lewy neurites alone, or diffuse or fine granular cytoplasmic staining lacking any focal aggregates, in sections immunohistochemically stained with anti-phosphorylated α-synuclein antibodies, following the revised Consensus Guidelines for DLB (22). PD with dementia was differentiated from DLB using the definition in the Consensus Guidelines: "dementia appears more than 12 months after the onset of parkinsonism" (21). In this study, we subcategorized our Stages I and II into primary and secondary α-synucleinopathy, based on our previous results (14, 15). Primary α-synucleinopathy (24) showed accentuation in the brainstem and spread to the spinal cord and was further subdivided into brainstem, transitional, and neocortical forms, according to the Lewy body score (21). Secondary α-synucleinopathy preferentially involved the amygdala and was termed the amygdala variant (25) in both Stage I (IA) and Stage II (IIA) (26).

The Adrenal Glands

The adrenal glands from all 783 cases were studied with hematoxylin and eosin staining and immunohistochemistry using monoclonal and polyclonal anti-phosphorylated α-synuclein antibodies. The immunoreactive structures were screened in the parenchyma as well as in the autonomic nerves or ganglia in the capsular fatty tissue.

Evaluation of Pathology Related to Other Disorders Presenting With Dementia or Parkinsonism

All 783 cases were evaluated with modified methenamine (16) and Gallyas-Braak silver (17) stainings as well as immunohistochemically using anti-phosphorylated tau

TABLE 2. Lewy Body-Related α-Synucleinopathy in the Central Nervous System and Adrenal Glands

LB Stage*	Type of Distribution/Diagnosis	PA	Dementia	Number of Cases	LBAS in the Adrenal Gland	Ratio (%)
0				577	1	0.2
0.5				36	1	2.8
I				85	14	16.5
	B			41	6	14.6
	T			35	8	22.9
	A			9	0	0
II				29	20	69
	B			5	4	80
	T			19	14	73.7
	N			2	2	100
	A			3	0	0
III	PD	+	−	4	4	100
IV				27	25	92.6
	PDDT	+	+	10	10	100
	DLBT			17	15	88.2
		+	+	7	7	100
		−	+	10	8	80
V				25	22	88
	PDDN	+	+	4	4	100
	DLBN			21	18	85.7
		+	+	7	7	100
		−	+	14	11	78.6
Total				783	87	11.1

*Lewy body stage (14, 15).

LB, Lewy body; PA, parkinsonism; LBAS, Lewy body-related α-synucleinopathy; B, brainstem; T, transitional; N, neocortical; A, amygdala variant; PD, Parkinson disease without dementia; PDDT, Parkinson disease with dementia, with a Lewy body score corresponding to the value for the transitional form; DLBT, dementia with Lewy bodies, with a Lewy body score corresponding to the value for the transitional form; PDDN, Parkinson disease with dementia, with a Lewy body score corresponding to the value for the neocortical form; DLBN, dementia with Lewy bodies, with a Lewy body score corresponding to the value for the neocortical form.

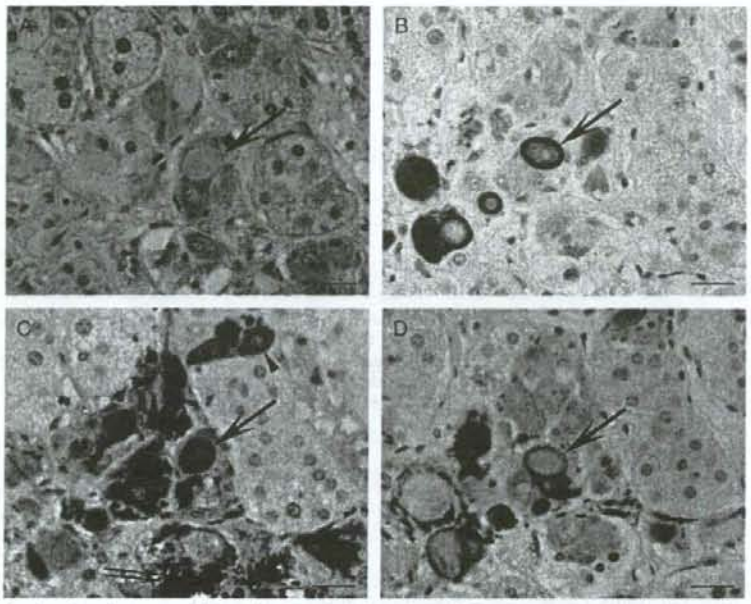

FIGURE 1. Lewy body-related α-synucleinopathy in the adrenal medulla. **(A)** Lewy bodies (arrow) are identified in a hematoxylin and eosin-stained section. **(B)** Anti-phosphorylated α-synuclein (Pser129) antibody clearly visualizes Lewy body-related inclusions, some of which show a central halo and a peripheral rim (arrow). This section is adjacent to that shown in **(A)**. **(C)** Anti-tyrosine hydroxylase immunohistochemistry demonstrates a positively stained cytoplasm of the ganglion cells (arrowhead) and Lewy bodies (arrow), in addition to adrenal medullary cells (double arrows). This section is adjacent to that shown in panel **(A)**. **(D)** Anti-phosphorylated neurofilament (SMI31) antibody intensely stained the periphery of some Lewy bodies (arrow). This section is a serial section of that shown in **(B)**. Scale bars = **(A–D)** 25 μm.

(AT8) and anti-β amyloid antibodies. Neurofibrillary tangles were classified into 7 stages as defined by Braak and Braak (27). Senile plaques were also stratified according to Braak and Braak (27) because this Braak stage was the only available stage for parenchymal deposition of β amyloid. Argyrophilic grains were classified into 4 stages as we have previously described (28).

A neurofibrillary tangle stage equal to or greater than IV and senile plaque stage C were adopted for the diagnosis of AD, as previously reported (29). Diagnoses of "dementia with grains" and the "neurofibrillary tangle-predominant form of dementia" were based on Jellinger's definitions (30, 31). A diagnosis of vascular dementia was based on the National Institute of Neurological Disorders and Stroke (NINDS)-Association Internationale pour la Recherche et l'Enseignement en Neurosciences (AIREN) criteria (32). A diagnosis of progressive supranuclear palsy was based on the NINDS diagnostic criteria (33), skipping the clinical inclusion scheme.

TABLE 3. Distribution of Lewy Body-Related α-Synucleinopathy in the Adrenal Gland Specimens

Region	Lewy Body-Related Pathology (Number)	Frequency (%)
Ganglia in the adrenal medulla	58	66.7
Nerve fascicles in the adrenal cortex	23	26.4
Ganglia in the periadrenal fatty tissue	37 (of 50 cases*)	(74.0)
Nerve fascicles in the periadrenal fatty tissue	81	93.1

*. Ganglia in the periadrenal fatty tissue were identified in 50 of the 87 cases.

Clinical Information

Clinical information, including the presence or absence of parkinsonism and autonomic failure, as well as an assessment of the patient's cognitive state, was obtained from medical charts. The entire collection of medical records, including neuroimages (magnetic resonance imaging, computed tomography, single photon emission computed tomography, and positron emission tomography) of the patients on whom an autopsy was performed, was stored in the TMGH's database. When the previous medical history of another hospital was available, the medical records from that hospital were also obtained with written informed consent from the patient's relatives. Scores from the Mini-Mental State Examination (34) or the Hasegawa Dementia Scale (35) or its revised version (36) and Instrumental Activities of Daily Living scale (37) were used to evaluate cognitive function.

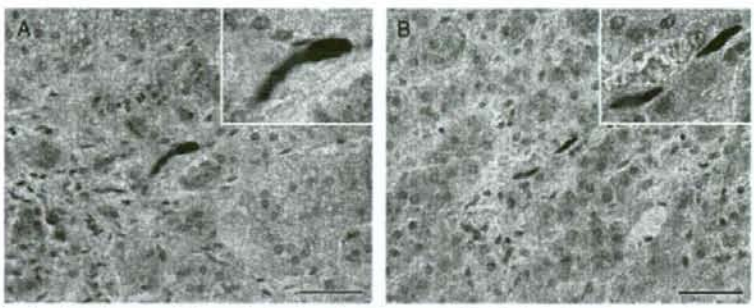

FIGURE 2. Lewy body-related α-synucleinopathy in the adrenal cortex. **(A, B)** Anti-phosphorylated α-synuclein antibody **(A)**, psyn#64, monoclonal; Pser129, polyclonal **(B)**. Both antibodies are raised against the same synthetic peptide and show the same specificity in immunoblots (15, 19). The polyclonal antibody presents less background than the monoclonal one in the peripheral autonomic nervous tissues examined and demonstrates positively stained thick neurites with focal swelling (the left inset). Scale bars = **(A, B)** 50 μm.

The Clinical Dementia Rating Scale (38) was retrospectively determined by 2 independent board-certified neurologists. If the resulting Clinical Dementia Rating Scale scores were in agreement, the score was accepted. If not, the neurologists reconciled their differences after interviews with the patient's attending physicians and caregivers. Locomotor activity was evaluated using the Barthel Index of Activity of Daily Living (39). Information about parkinsonism, tremor (resting), rigidity (cogwheel), bradykinesia, and postural instability was extracted from the records of neurologic examinations, and the presence of more than 2 of these symptoms was interpreted as positive for parkinsonism. To assess autonomic failure, documentation of orthostatic hypotension was retrieved from the charts. There were limitations in clinical assessment in this retrospective manner, compared with prospective clinical studies, but we made efforts to decrease the gap, using the merit of community-based settings. The majority of the cases had long-term follow-up (up to more than 40 years) and both cognitive and motor function parameters were routinely evaluated at each admission to TMGH. The majority of the relatives who approved the autopsy were also medically followed by the TMGH, and we tried to have direct interviews with them to confirm descriptions in clinical charts.

Statistical Analysis

Statistical analysis was performed using the chi-square test or the Fisher exact test for comparisons of categorical data. Statistical significance was set at $p < 0.05$.

RESULTS

Incidence and Distribution of Lewy Body-Related α-Synucleinopathy in the Adrenal Glands

LBAS was found in 207 (26.4%) of 783 cases examined. Among them, 87 cases (11.1%) (Table 2) showed LBAS in the following areas of sections of the adrenal glands: 1) sympathetic ganglion cells in the adrenal medulla (Fig. 1); 2) sympathetic nerve fascicles in the interstitial tissue of the adrenal cortex (Fig. 2); 3) sympathetic ganglia in the fatty tissue surrounding the adrenal capsule (Fig. 3); and 4) nerve fascicles in the fatty tissue surrounding the adrenal capsule (Fig. 4). The above 4 structures were immunoreactive for anti-TH antibody, a marker of the sympathetic nervous system (Figs. 1C and 3C). The regional distribution of LBAS is summarized in Table 3.

So-called "adrenal bodies" (40) were always negative for anti-phosphorylated α-synuclein antibodies (data not shown). SMI31 stained preserved unmyelinated fibers of TH-immunoreactive nerve fascicles in all of the cases with adrenal LBAS, including PD cases, in contrast to a marked decrease in TH-immunoreactive unmyelinated fibers in the pericardium in these cases (data not shown) (9, 10).

Comparison With the Lewy Body Stage in the Central Nervous System

The correlation between the Lewy body stage in the central nervous system and the presence or absence of α-synucleinopathy in the adrenal gland is summarized in Table 2. Lewy bodies were found in one Lewy body Stage 0 case and in one Lewy body Stage 0.5 case. All of the PD cases with or without dementia had LBAS in the adrenal gland.

To elucidate the initial stage of LBAS, the percentage of cases with positive anti-phosphorylated α-synuclein immunoreactivity in the adrenal glands was estimated in each subgroup of Lewy body Stage I and Stage II (Table 2). None of the amygdala variants exhibited anti-phosphorylated α-synuclein immunoreactivity in the adrenal glands. In contrast, nearly 20% of Stage I and approximately 80% of Stage II cases of the primary α-synucleinopathy presented with LBAS in the adrenal glands.

We further analyzed Lewy body Stage IV and Stage V cases (n = 5) that did not present with Lewy body-related pathology in the adrenal glands. These cases had no clinical description of Parkinsonism or orthostatic hypotension. Four of these cases were complicated by AD pathology (changes in senile plaque stage C and an neurofibrillary tangle stage

equal to or greater than Stage III), and the fifth case was complicated by argyrophilic grain Stage III. All 14 DLB cases with a clinical description of parkinsonism and all 8 DLB cases with no such description but with other mild senile changes presented with adrenal LBAS. However, the 7 DLB cases with similar Alzheimer pathology and the 3 DLB cases with argyrophilic grain Stage III contained adrenal Lewy body pathology and did not show easily detectable morphologic differences from the above mentioned 5 cases without the adrenal Lewy body pathology.

Clinicopathologic Correlation With Lewy Body Pathology in the Adrenal Glands

Orthostatic hypotension was clinically described in the medical records for 6 of the 783 cases. Five of these cases showed LBAS in the adrenal glands: one case of PD without clinical description of dementia, one case of PD with dementia with the Lewy score of the transitional form, one case of PD with dementia with the Lewy score of the neocortical form, and 2 cases with DLB transitional form. Of the 2 cases in which Lewy bodies were restricted to the adrenal glands, one case with Lewy body Stage 0.5 clinically presented with syncope-like attack, but there was no definite evidence of orthostatic hypotension.

DISCUSSION

Our studies represent the first demonstration in the literature of the following. 1) LBAS always involved the adrenal gland in PD, with or without dementia. 2) Adrenal glands were always free of LBAS in cases with the amygdala variant. 3) DLB cases that lacked LBAS in the adrenal glands were always complicated by the presence of moderate to severe Alzheimer pathology or argyrophilic grain disease and had no clinical description of parkinsonism. 4) LBAS in the adrenal glands can occur independently of LBAS in the central nervous system. Thus, the immunohistochemical evaluation of adrenal glands with anti-phosphorylated α-synuclein antibodies can be used to evaluate Lewy body pathology involving the peripheral autonomic nervous system.

Lewy bodies and their related structures are present in the adrenal glands of patients with PD or DLB (13, 41). However, the detection ratio was only approximately 30% (41), which differed from the ratio in the sympathetic ganglia (42), in which Lewy bodies were always present in patients with PD or DLB. In the present study we were able to detect Lewy body-related pathology immunohistochemically in adrenal glands or their associated sympathetic tissues with anti-phosphorylated α-synuclein antibodies in

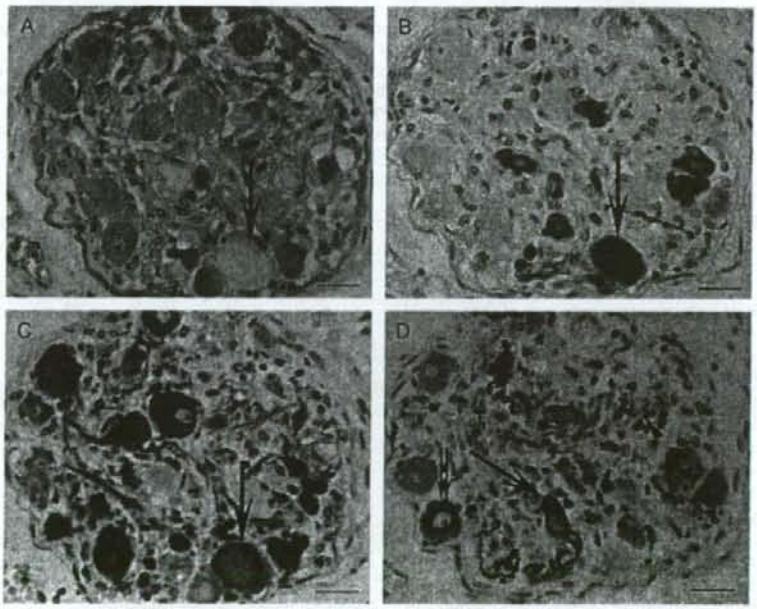

FIGURE 3. Lewy body-related α-synucleinopathy in a sympathetic ganglion from the fatty tissue surrounding the adrenal capsule. **(A)** Lewy bodies (arrow) are visible in a hematoxylin and eosin-stained section. **(B)** Anti-phosphorylated α-synuclein (Pser129) immunostaining visualizes the abundant Lewy body-related α-synucleinopathy (arrow). This image represents a serial section of that shown in **(A)**. **(C)** Anti-tyrosine hydroxylase staining in the neuronal cytoplasm, neurites, and Lewy bodies (arrow). This image is a serial section of that shown in **(B)**. **(D)** Anti-phosphorylated neurofilament antibody (SMI31) reveals axons (arrowheads) and some neuronal perikarya (double arrows). The periphery of some Lewy bodies (arrow) is intensely stained by the antibody. Scale bars = **(A–D)** 25 μm.)

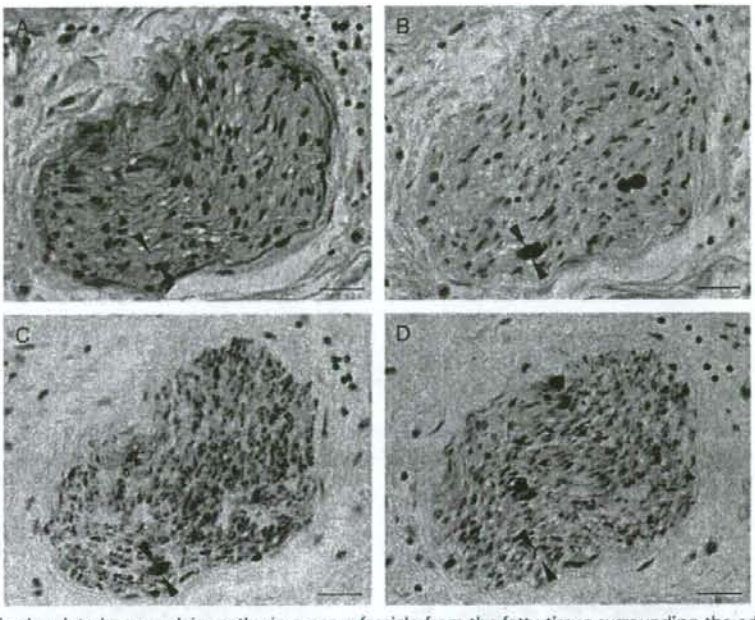

FIGURE 4. Lewy body-related α-synucleinopathy in a nerve fascicle from the fatty tissue surrounding the adrenal capsule. **(A)** An axonal pale body (arrowheads) is detectable with hematoxylin and eosin staining. **(B)** Anti-phosphorylated α-synuclein antibody (psyn#64) stains the pale body (arrowheads). Lewy dots are also visualized by the antibody. This image is a serial section of that shown in **(A)**. **(C)** Anti-tyrosine hydroxylase antibody clearly visualizes the pale body (arrowheads) as well as adjacent axons in the fascicle. This image is a serial section of that shown in **(B)**. **(D)** Anti-phosphorylated neurofilament antibody (SMI31) stains the periphery of the pale body (arrowheads) as well as axons of the nerve fascicle. This image is a serial section of that shown in **(C)**. Scale bars = **(A–D)** 25 μm.

all cases of PD. Because adrenal glands are routine sites of investigation in general autopsy, our results indicate that evaluation of the peripheral autonomic nervous system in Lewy body disease is possible through the examination of archival paraffin blocks of adrenal glands. Pathologic examination in TMGH requires strict removal of fatty tissue from adrenal glands to evaluate their exact weight. When such removal is not done, the detection rate of periadrenal paraganglia was almost 100% (Dr. K. Kawabata, Director, Department of Pathology, Akashi City Hospital, personal communication, 2006). Because the periadrenal retroperitoneal space contains abundant paraganglia and associated sympathetic ganglia and nerves, even the very thin surrounding tissue of the adrenal glands in our series always included useful peripheral sympathetic nervous tissue.

Adrenal glands are frequently affected by autolysis, inflammation, or metastasis, but our study suggests that the organs and the surrounding sympathetic ganglia and nerves are nevertheless useful for assessing morphologic changes in the peripheral autonomic nervous system in PD or DLB.

The amygdala variant of α-synucleinopathy is complicated by either a severe burden of tangles and plaques or by argyrophilic grains in the amygdala. This type of α-synucleinopathy is associated with AD and Down syndrome (25, 26, 43, 44), as well as with other tauopathies (45). We termed this type "secondary" (14, 15). The present study clearly shows that immunopathologic studies of the adrenal glands can distinguish secondary α-synucleinopathy from PD.

Braak et al (46) proposed a staging system for α-synucleinopathy in the brains of a nondemented general cohort and in cases of PD. Our series, with a cohort having a mean age of approximately 80 years, included a high percentage of dementia, as was expected. The differential diagnosis between DLB and PD with dementia is often difficult in such aged cohorts. Thus, Braak et al's staging paradigm could not be applied effectively to our group (15). We always examined the spinal cord, a structure not included in Braak et al's staging, to evaluate the preganglionic sympathetic neurons. Our results show that some DLB cases, whose α-synucleinopathy definitely involved sympathetic preganglionic neurons, did not present with α-synucleinopathy in the adrenal or periadrenal tissues. All of these cases met the morphologic criteria for AD from the elderly cohort (47) or for dementia with grains (28) and lacked a clinical description of parkinsonism. However, many other cases of DLB, complicated by similar changes in AD or dementia with grains and lacking a clinical description of parkinsonism, presented with α-synucleinopathy involving the adrenal or periadrenal tissues. Although

morphologic differences in the Lewy body pathology in the central nervous system at the final stage of the illness may become unclear, the pathologic examination of LBAS in the peripheral autonomic nervous system could delineate those DLB cases complicated by other senile changes and presenting with a limbic-neocortical-dominant distribution of Lewy body pathology, lesser involvement of the brainstem and spinal cord, and a lack of adrenal and periadrenal Lewy body pathology from other DLB cases with a pathology more common to PD (with or without dementia), which always presents with adrenal or periadrenal Lewy body pathology.

Although the number of cases was small, 2 cases presented with Lewy bodies only in the adrenal glands and lacked Lewy bodies in the central nervous system. These cases could possibly represent the earliest stage of Lewy body-related progressive autonomic failure. From the points of disease pathogenesis and hierarchy of the Lewy body disorders, this result indicates that the adrenal gland could be the initial and primary target for these progressive disorders.

In the present study, we retrospectively investigated the correlation between clinical and pathologic presentations of adrenal glands. Although there were definite limitations in our study based on the review of medical records, the observed Lewy body-related pathology involving adrenal tissues did not correspond to any symptomatology of adrenal insufficiency, except for orthostatic hypotension. Also, our studies did not indicate how to detect this adrenal or periadrenal Lewy body-related pathology in clinical testing. Reduced uptake of MIBG in cardiac scintigraphy in Lewy body disease corresponds to decreased TH-immunoreactivity as well as to α-synucleinopathy in unmyelinated fibers from the epicardial fatty tissue of the anterior wall of the left ventricle of the heart (8–10). However, because the TH-immunoreactive unmyelinated fibers in the periadrenal fatty tissue were relatively preserved in this study, MIBG scintigraphy, which is also used for the detection of pheochromocytoma of the adrenal glands, may not be useful for detection of this Lewy body-related pathology in adrenal tissues. Therefore, we are now planning a prospective functional study of cases with Lewy body disease consisting of the tilt test and simultaneous blood sampling to gauge the serum noradrenalin level, as well as the resting adrenalin level, to detect this adrenal pathology clinically.

In conclusion, the immunohistochemical examination of adrenal glands with anti-phosphorylated α-synuclein antibodies can help differentiate the primary and the secondary forms of LBAS, as well as identify where LBAS starts in the human body and how it spreads.

ACKNOWLEDGMENTS

We thank Mr. Naoo Aikyo, Ms. Mieko Harada, and Ms. Nobuko Naoi (Department of Neuropathology, Tokyo Metropolitan Institute for Gerontology) for the preparation of sections and Dr. Kinuko Suzuki (Department of Pathology and Laboratory Medicine, University of North Carolina at Chapel Hill) for helpful discussions. We also thank two anonymous neurologists for preparing the Clinical Dementia Rating scores used in this study.

REFERENCES

1. Kosaka K. Dementia and neuropathology in Lewy body disease. Adv Neurol 1993;60:456–63
2. Kosaka K, Yoshimura M, Ikeda K, Budka H. Diffuse type of Lewy body disease: Progressive dementia with abundant cortical Lewy bodies and senile changes of varying degree-a new disease? Clin Neuropathol 1984;3:185–92
3. Koike Y, Takahashi A. Autonomic dysfunction in Parkinson's disease. Eur Neurol 1997;38(Suppl 2):8–12
4. Horimoto Y, Matsumoto M, Akatsu H, et al. Autonomic dysfunctions in dementia with Lewy bodies. J Neurol 2003;250:530–33
5. Hishikawa N, Hashizume Y, Yoshida M, Sobue G. Clinical and neuropathological correlates of Lewy body disease. Acta Neuropathol (Berl) 2003;105:341–50
6. Hakusui S, Yasuda T, Yanagi T, et al. A radiological analysis of heart sympathetic functions with meta-[^{123}I]iodobenzylguanidine in neurological patients with autonomic failure. J Auton Nerv Syst 1994;49:81–84
7. Orimo S, Ozawa E, Nakade S, Sugimoto T, Mizusawa H. (^{123})I-metaiodobenzylguanidine myocardial scintigraphy in Parkinson's disease. J Neurol Neurosurg Psychiatry 1999;67:189–94
8. Orimo S, Oka T, Miura H, et al. Sympathetic cardiac denervation in Parkinson's disease and pure autonomic failure but not in multiple system atrophy. J Neurol Neurosurg Psychiatry 2002;73:776–77
9. Orimo S, Amino T, Takahashi A, et al. Cardiac sympathetic denervation in Lewy body disease. Parkinsonism Relat Disord 2006;12:S99–105
10. Mitsui J, Saito Y, Momose T, et al. Pathology of the sympathetic nervous system corresponding to the decreased cardiac uptake in ^{123}I-metaiodobenzylguanidine (MIBG) scintigraphy in a patient with Parkinson disease. J Neurol Sci 2006;243:101–4
11. Yoshita M, Taki J, Yokoyama K, et al. Value of ^{123}I-MIBG radioactivity in the differential diagnosis of DLB from AD. Neurology 2006;66:1850–54
12. Forno LS, Sternberger LA, Sternberger NH, Strefling AM, Swanson K, Eng LF. Reaction of Lewy bodies with antibodies to phosphorylated and non-phosphorylated neurofilaments. Neurosci Lett 1986;64:253–58
13. Wakabayashi K, Takahashi H. Neuropathology of autonomic nervous system in Parkinson's disease. Eur Neurol 1997;38(Suppl 2):2–7
14. Saito Y, Kawashima A, Ruberu NN, et al. Accumulation of phosphorylated α-synuclein in aging human brain. J Neuropathol Exp Neurol 2003;62:644–54
15. Saito Y, Ruberu NN, Sawabe M, et al. Lewy body-related α-synucleinopathy in aging. J Neuropathol Exp Neurol 2004;63:742–49
16. Yamaguchi H, Haga C, Hirai S, Nakazato Y, Kosaka K. Distinctive, rapid, and easy labeling of diffuse plaques in the Alzheimer brains by a new methenamine silver stain. Acta Neuropathol 1990;79:569–72
17. Gallyas F. Silver staining of Alzheimer's neurofibrillary changes by means of physical development. Acta Morphol Acad Sci Hung 1971;19:1–8
18. Saito Y, Nakahara K, Yamanouchi H, Murayama S. Severe involvement of ambient gyrus in dementia with grains. J Neuropathol Exp Neurol 2002;61:789–96
19. Fujiwara H, Hasegawa M, Dohmae N, et al. α-Synuclein is phosphorylated in synucleinopathy lesions. Nat Cell Biol 2002;4:160–64
20. Jakes R, Crowther RA, Lee VM, Trojanowski JQ, Iwatsubo T, Goedert M. Epitope mapping of LB509, a monoclonal antibody directed against human α-synuclein. Neurosci Lett 1999;269:13–16
21. McKeith IG, Galasko D, Kosaka K, et al. Consensus guidelines for the clinical and pathologic diagnosis of dementia with Lewy bodies (DLB): Report of the consortium on DLB international workshop. Neurology 1996;47:1113–24
22. McKeith IG, Dickson DW, Lowe J, et al. Diagnosis and management of dementia with Lewy bodies: Third report of the DLB Consortium. Neurology 2005;65:1863–72
23. Dickson DW, Schmidt ML, Lee VM, Zhao ML, Yen SH, Trojanowski JQ. Immunoreactivity profile of hippocampal CA2/3 neurites in diffuse Lewy body disease. Acta Neuropathol (Berl) 1994;87:269–76

24. Forman MS, Schmidt ML, Kasturi S, Perl DP, Lee VM, Trojanowski JQ. Tau and α-synuclein pathology in amygdala of Parkinsonism-dementia complex patients of Guam. Am J Pathol 2002;160:1725–31
25. Uchikado H, Lin WL, DeLucia MW, Dickson DW. Alzheimer disease with amygdala Lewy bodies: A distinct form of α-synucleinopathy. J Neuropathol Exp Neurol 2006;65:685–97
26. Hamilton RL. Lewy bodies in Alzheimer's disease: A neuropathological review of 145 cases using α-synuclein immunohistochemistry. Brain Pathol 2000;10:378–84
27. Braak H, Braak E. Neuropathological staging of Alzheimer-related changes. Acta Neuropathol 1991;82:239–59
28. Saito Y, Ruberu NN, Sawabe M, et al. Staging of argyrophilic grains: An age-associated tauopathy. J Neuropathol Exp Neurol 2004; 63:911–18
29. Murayama S, Saito Y. Neuropathological diagnostic criteria for Alzheimer's disease. Neuropathology 2004;24:254–60
30. Jellinger KA. Dementia with grains (argyrophilic grain disease). Brain Pathol 1998;8:377–86
31. Jellinger KA, Bancher C. Senile dementia with tangles (tangle predominant form of senile dementia). Brain Pathol 1998;8:367–76
32. Roman GC, Tatemichi TK, Erkinjuntti T, et al. Vascular dementia: Diagnostic criteria for research studies. Report of the NINDS-AIREN International Workshop. Neurology 1993;43:250–60
33. Hauw JJ, Daniel SE, Dickson D, et al. Preliminary NINDS neuropathologic criteria for Steele-Richardson-Olszewski syndrome (progressive supranuclear palsy). Neurology 1994;44:2015–19
34. Folstein MF, Folstein SE, McHugh PR. "Mini-mental state": A practical method for grading the cognitive state of patients for the clinician. J Psychiatr Res 1975;12:189–98
35. Hasegawa K, Inoue K, Moriya K. An investigation of dementia rating scale for the elderly (in Japanese). Seishin Igaku 1974;16:965–69
36. Katoh S, Simogaki H, Onodera A, et al. Development of the revised version of Hasegawa's dementia scale (HDS-R). Rounen Seishinigaku Zashi 1991;2:1339–47
37. Lawton MP, Brody EM. Assessment of older people: self-maintaining and instrumental activities of daily living. Gerontologist 1969;9:179–86
38. Hughes CP, Berg L, Danziger WL, Coben LA, Martin RL. A new clinical scale for the staging of dementia. Br J Psychiatry 1982;140: 566–72
39. Mahoney FI, Barthel DW. Functional evaluation: The Barthel Index. Md State Med J 1965;14:61–65
40. Kimula Y, Utsuyama M, Yoshimura M, Tomonaga M. Element analysis of Lewy and adrenal bodies in Parkinson's disease by electron probe microanalysis. Acta Neuropathol (Berl) 1983;59:233–36
41. Wakabayashi K, Takahashi H, Ohama E, Takeda S, Ikuta F. Lewy bodies in the visceral autonomic nervous system in Parkinson's disease. Adv Neurol 1993;60:609–12
42. Forno LS, Norville RL. Ultrastructure of Lewy bodies in the stellate ganglion. Acta Neuropathol (Berl) 1976;34:183–97
43. Lippa CF, Fujiwara H, Mann DM, et al. Lewy bodies contain altered α-synuclein in brains of many familial Alzheimer's disease patients with mutations in presenilin and amyloid precursor protein genes. Am J Pathol 1998;153:1365–70
44. Lippa CF, Schmidt ML, Lee VM, Trojanowski JQ. Antibodies to α-synuclein detect Lewy bodies in many Down's syndrome brains with Alzheimer's disease. Ann Neurol 1999;45:353–57
45. Yamazaki M, Arai Y, Baba M, et al. α-Synuclein inclusions in amygdala in the brains of patients with the parkinsonism-dementia complex of Guam. J Neuropathol Exp Neurol 2000;59:585–91
46. Braak H, Del Tredici K, Rub U, de Vos RA, Jansen Steur EN, Braak E. Staging of brain pathology related to sporadic Parkinson's disease. Neurobiol Aging 2003;24:197–211
47. Knopman DS, Parisi JE, Salviati A, et al. Neuropathology of cognitively normal elderly. J Neuropathol Exp Neurol 2003;62:1087–95

Granular Tau Oligomers as Intermediates of Tau Filaments†

Sumihiro Maeda,‡ Naruhiko Sahara,‡ Yuko Saito,§ Miyuki Murayama,‡ Yuji Yoshiike,‡ Hyonchol Kim,⊥ Tomohiro Miyasaka,‡ Shigeo Murayama,§ Atsushi Ikai,∥ and Akihiko Takashima*,‡

Lab for Alzheimer's Disease, RIKEN Brain Science Institute, 2-1 Hirosawa, Wako, Saitama 351-0198, Japan, Department of Neuropathology and Department of Pathology, Tokyo Metropolitan Institute of Gerontology, Tokyo Metropolitan Geriatric Hospital, 35-2 Sakaecho, Itabashi-ku, Tokyo 173-0015, Japan, and Department of Life Science, Graduate School of Bioscience and Biotechnology, Tokyo Institute of Technology, 4259 Nagatsuda, Midori-ku, Yokohama, Kanagawa 226-8501, Japan

Received July 6, 2006; Revised Manuscript Received December 15, 2006

ABSTRACT: Neurofibrillary tangles (NFTs) are pathological hallmarks of several neurodegenerative disorders, including Alzheimer's disease (AD). NFTs are composed of microtubule-binding protein tau, which assembles to form paired helical filaments (PHFs) and straight filaments. Here we show by atomic force microscopy that AD brain tissue and in vitro tau form granular and fibrillar tau aggregates. CD spectral analysis and immunostaining with conformation-dependent antibodies indicated that tau may undergo conformational changes during fibril formation. Enriched granules generated filaments, suggesting that granular tau aggregates may be an intermediate form of tau fibrils. The amount of granular tau aggregates was elevated in prefrontal cortex of Braak stage I cases compared to that of Braak stage 0 cases, suggesting that granular tau aggregation precedes PHF formation. Thus, granular tau aggregates may be a relevant marker for the early diagnosis of tauopathy. Reducing the level of these aggregates may be a promising therapy for tauopathies and for promoting healthy brain aging.

Neurofibrillary tangles (NFTs)[1] are common in many neurodegenerative diseases and to some degree in normal aging (*1*, *2*). NFTs are intracellular neuronal clusters of fibrils that consist of paired helical filaments (PHFs) and straight filaments (SFs). These filaments are composed of hyperphosphorylated tau, a type of microtubule-binding protein. Some have proposed a connection between NFT formation and neuronal loss, because NFTs are observed in brain regions that also exhibit neuronal loss (*3*). Recent genetic studies of frontotemporal dementia with parkinsonism linked to chromosome 17 (FTDP-17) revealed that a mutation in the tau gene induces NFT formation and neuronal loss (*4*), suggesting that tau dysfunction itself could lead to NFT formation and neuronal loss.

It is unclear, however, how tau forms fibrils and how tau contributes to neurodegeneration. A recent report showed that inhibiting tau expression in tau transgenic mice protected against neuronal death, even though NFTs were still produced (*5*). These results suggest that the degenerating pathway, triggered by tau overexpression, may branch from a tau filament formation pathway. Tau may produce toxic aggregates before forming tau fibrils.

Tau fibril formation has been studied extensively in vitro. Anionic surfactants accelerate fibril formation of tau protein in vitro (*6*). Fibril formation can be monitored by thioflavin fluorescence, which recognizes aggregations having a β-sheet conformation. In this study, together with the thioflavin assay, we applied atomic force microscopy (AFM) to tau in solution to track structural changes in tau and to identify intermediates of tau filaments.

MATERIALS AND METHODS

Expression and Purification of Recombinant Tau Protein. Recombinant human tau (2N4R) in the pRK172 vector was purified using methods described previously (*7*) with some modifications. Details of these methods are described in the Supporting Information. After being freeze-dried, tau was dissolved in water and stored as a stock solution at −30 °C.

Incubation of Tau and Fluorescence Spectroscopy (ThT assay). The degree of tau aggregation was determined using thioflavin T (ThT) (*8*). Tau or BSA (control protein) stock solutions were diluted to 10 μM with 10 mM HEPES (pH 7.4), 100 mM NaCl, 10 μM heparin, and 10 μM ThT (final volume of 50 μL per well) and incubated in a damp box at 37 °C. At indicated time points (see Figure 2), we measured ThT fluorescence levels as previously described (*9*).

Atomic Force Microscopy (AFM). A multimode Nanoscope IIIa (Digital Instruments, Santa Barbara, CA) equipped

† This work is partly supported by a Grant-in-Aid for Scientific Research (11680746, from the Japanese Ministry of Education, Science, and Culture) and Promotion of Novel Interdisciplinary Fields Based on Nanotechnology and Materials.

* To whom correspondence should be addressed. E-mail: kenneth@brain.riken.jp. Telephone: +81-(0)48-467-9627. Fax: +81-(0)48-467-5916.

‡ RIKEN Brain Science Institute.

§ Tokyo Metropolitan Geriatric Hospital.

∥ Tokyo Institute of Technology.

⊥ Present address: Department of Biomedical Information, Division of Biosystems, Institute of Biomaterials and Bioengineering, Tokyo Medical and Dental University, 2-3-10 Surugadai, Chiyoda-ku, Tokyo 101-0062, Japan.

[1] Abbreviations: NFT, neurofibrillary tangle; PHF, paired helical filament; SF, straight filament; FTDP-17, frontotemporal dementia with parkinsonism linked to chromosome 17; AFM, atomic force microscopy; dLLS, dynamic laser light scattering; sLLS, static laser light scattering; CD, circular dichroism; ThT, thioflavin T; BSA, bovine serum albumin.

10.1021/bi061359o CCC: $37.00
Published on Web 03/06/2007

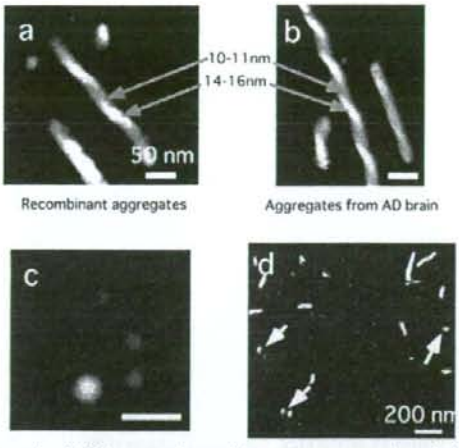

FIGURE 1: AFM images of recombinant tau aggregates in solution, fibrils (a) and granules (c). AFM images of PHFs and straight filaments purified from an AD brain (b). The heights of "mountains and valleys" of the twisted filaments are indicated. Tau-enriched fractions from the AD brain contain tau fibrils and granules (arrow) (d). Scale bars are 50 (a−c) and 200 nm (d).

with tapping mode was used for AFM observations in solution. An OMCL-TR400PSA device (Olympus) was used as a microcantilever. Incubated tau solutions from three different Black Cliniplate wells were combined, dropped onto freshly cleaved mica, allowed to set for 10 min, and then examined via AFM. For human tau, samples were left on the mica surface for 30 min and washed once with buffer prior to AFM assessment. We processed the height images of structures using NIH-image 1.62 and calculated the major (length) and minor (diameter) axes for each particle. Data from four different regions (4 μm^2) of each structure were plotted.

Sucrose Step Gradients and Preparation of Concentrated Tau. An incubated or immunoaffinity-purified tau solution (1 mL) was fractionated using discontinuous sucrose gradients using a TLA 55 rotor (Beckman) on a 5 mL scale as described previously (*10*). To concentrate the fractions and for buffer exchanges with 10 mM HEPES and 100 mM NaCl, we filtered the fractions using Centricut mini filters (10 kDa cutoff; KURABOU) at room temperature for 1 or 2 days. Although granular tau oligomers are insoluble in sarcosyl (Figure 1 of the Supporting Information), most remained in the supernatant fraction after ultracentrifugation (100Kg for 30 min) because of their small sedimentation coefficient. Centrifuging the supernatant fraction at 200Kg for 2 h, however, successfully separated the oligomers from soluble and flexible tau species.

Dot Blot Analysis. The tau protein concentration in each fraction was determined using amino acid hydrolysis, and the same amount of tau was dotted onto nitrocellulose membranes. We used the following primary antibodies: E1 (recognizes total tau), MC1 (recognizes PHF tau conformational change; generous gift from P. Davies, Albert Einstein College of Medicine, Bronx, NY), and A11 (recognizes the conformation of toxic Aβ; Biosource) (*11*). The membranes were incubated with peroxidase-labeled secondary antibody and visualized using ECL.

Laser Light Scattering and Circular Dichroism Spectroscopy. The buffers from fractions 1 and 3 were exchanged with high-salt buffer [10 mM Tris (pH 7.4) and 800 mM NaCl] to minimize further aggregation. To ensure the elimination of filaments formed in the filtering step, the sample was centrifuged at 100Kg for 30 min at 4 °C. After we had confirmed that the granular aggregates were not filamentous using AFM, the tau oligomeric fraction was subjected to static and dynamic laser light scattering using a Zetasizer (Sysmex) at 23 °C. The molecular mass of granular tau oligomer was calculated as the average of triplicate experiments.

We measured the circular dichroism (CD) spectra of each fraction with a J-720 spectropolarimeter (Jasco). Samples placed in a cuvette with a path length of 1 mm were measured from 200 to 260 nm at 23 °C. Spectra obtained from an average of 20 scans were converted to mean residue ellipticity.

Human Brain Sample Preparation. Granular tau oligomer fractions from human brains were purified according to procedures described previously (*10*). Significant differences between each Braak stage were tested with the Kruskal Wallis test. Data were analyzed with InStat 3 for Macintosh (Graphpad, San Diego, CA).

RESULTS

Assessing the Formation of Filaments and Granules by AFM. AFM examination of a tau solution incubated for 72 h revealed the presence of twisted filaments (Figure 1a) resembling PHFs (Figure 1b). This experimental system allowed us to observe both filament and granule formation (Figure 1a,c). AFM examination of immunoaffinity-purified tau from AD brains revealed granules that are the same size as those observed in the in vitro tau aggregation system (Figure 1d). Granules and tau filaments were insoluble in *N*-lauroylsarcosine (sarcosyl) detergent (Figure 1 of the Supporting Information). These observations suggest that tau aggregates may form two different structures, granules and fibrils, both in vitro and in vivo.

Granule Formation Precedes Filament Formation. To understand the relationship between these different tau aggregates, we investigated how tau assembly in vitro changes over time by measuring ThT fluorescence and by using AFM. During the first incubation period of 4 h, ThT fluorescence levels remained constant and no aggregates were observed via AFM (Figure 2a of the Supporting Information). After incubation for 4 h, however, ThT fluorescence levels increased and spherically or elliptically shaped granules and fibrils formed (Figure 2a,b of the Supporting Information). We used the major-to-minor axis ratio to define granules ($1 \leq$ major-to-minor axis ratio < 2) and fibrils ($2 \leq$ major-to-minor axis ratio) and then determined temporal changes in ThT fluorescence (Figure 2). At incubation for 6 h, granule levels increased rapidly, reaching a plateau at 21 h. After incubation for 21 h, even though the levels of granular tau oligomers had plateaued, tau fibrils continued to grow. The number and length of fibrils continued to increase with incubation times of up to 328 h, reaching lengths of up to 950 nm and diameters of 15−25 nm (Figure 2c of the Supporting Information).

ThT fluorescence intensity seemed to correspond to both granular and fibrillar tau levels, suggesting that both granules

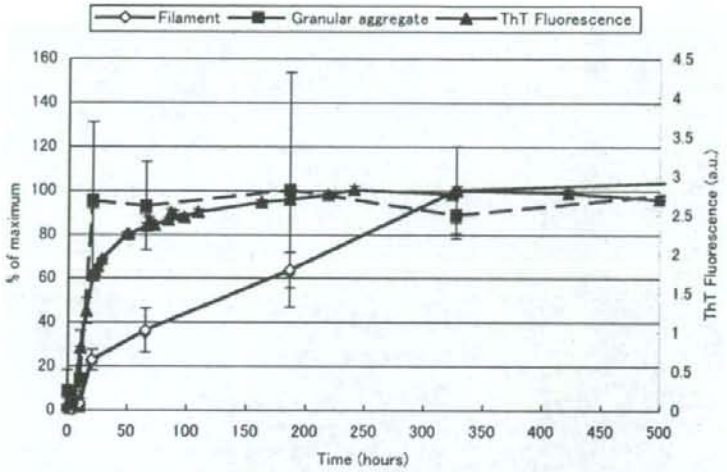

FIGURE 2: Temporal changes in ThT fluorescence and in granular tau oligomer and tau fibril levels. The ThT fluorescence of tau aggregation was measured at the indicated time points (mean ± standard deviation; $n = 3$). Tau granule and fibril levels were determined by calculating the area occupied from AFM images of tau samples taken at each time point (Figure 2b,c of the Supporting Information). Data are represented as percentages of the maximum oligomer and fibril levels (mean ± standard deviation).

and fibrils may possess a β-sheet conformation. These results led us to conclude that the granular tau oligomer might represent an intermediate form of tau fibril.

Characterization of Granular Tau Aggregates. We characterized granular tau aggregates by separating granular tau oligomers from the tau aggregate mixture. We then fractionated the incubated sample using sucrose gradient ultracentrifugation (Figure 3a). While fraction 1 contained no apparent aggregate, fraction 3 contained the largest amounts of granular tau oligomers. The size of granules in fraction 3 was normally distributed, with the largest sizes reaching 15−25 nm, as determined by AFM. Fractions 4−6 contained filaments. Since we could not assess by AFM the contamination of fraction 3 with soluble tau, we employed dynamic laser light scattering (dLLS) to assess soluble tau. dLLS analysis of fraction 3 revealed a single-peak distribution distinct from that of soluble tau (Figure 3b). Therefore, we concluded that fraction 3 does not contain fibrils or soluble tau but instead contains granular tau aggregates.

The temporal change of tau levels in each fraction was investigated using CBB staining after electrophoresis. In fraction 1 (soluble tau fraction), the amount of tau was reduced, corresponding to an increasing level of granular tau oligomer and fibril formation; tau levels in fraction 3 (granular tau oligomer fraction) decreased at later stages of the incubation, while the tau level in fraction 6 (filament fraction) continuously increased (Figure 3 of the Supporting Information). This result supports the observation under AFM that granular tau oligomer may be an intermediate form for tau filament.

We used fraction 3 to determine an approximate molecular mass of the granular tau oligomer. Figure 3c shows a Debye plot obtained from static laser light scattering (sLLS) analysis of granular oligomeric tau. The KC/RoP value at the y-intercept (sample concentration of zero) equals the reciprocal of the approximate molecular mass of the granular tau oligomer (Figure 3c). The approximate molecular mass of the granular tau oligomer averaged 1843.3 ± 112.4 kDa (average ± standard deviation; $n = 3$ replications), corresponding to 40 ± 3 tau molecules. KC/RoP values decreased as the sample concentration increased; that is, the granular tau oligomer has a negative second virial coefficient indicative of adhesive properties (*12*).

Conformational Differences between Granular and Fibrillar Tau. We used circular dichroism (CD) spectral analysis to analyze structural differences between soluble (fraction 1), granular oligomeric (fraction 3), and fibrillar forms (pellet, fraction 6) of tau. The spectral curve of fraction 1 had a minimum ellipticity of approximately 200 nm, indicating a random coil structure (*13*). Fibrillar tau (fraction 6) had fewer random coil structures and a growing "shoulder" in the curve at ~220 nm, indicating β-sheet structure. The CD spectrum of the granular tau oligomer (fraction 3) also revealed a shoulder smaller than that of fibrillar tau at ~220 nm (Figure 3d). The CD spectrum of granular tau oligomers was distinct but intermediate in form compared to those of soluble and fibrillar tau, suggesting that the granular tau oligomer may represent an intermediate structure. This observation was confirmed by probing samples of each tau fraction with conformation-dependent antibodies (Figure 3e). E1 antibody, which recognizes the N-terminus of tau, immunostained all fractions to the same extent. MC1, which recognizes a conformational change in PHF, did not immunostain the soluble tau fraction (fraction 1) but did immunostain granular and fibrillar tau fractions (fractions 2−6). A11 antibody, which recognizes toxic oligomers of β-amyloid, immunostained only fibrillar fractions (fractions 4−6). Taken together, these results indicate that tau fibrils might have another conformational form having an additional structure distinct from that of granular tau oligomer.

Conversion of Granular Aggregates into Filaments. To examine whether granular tau aggregates could form filaments, we enriched the concentration of tau by filtering fractions 1 and 3. Samples containing enriched granular tau oligomer formed filaments (Figure 4c,d), while samples containing enriched soluble tau failed to form aggregates

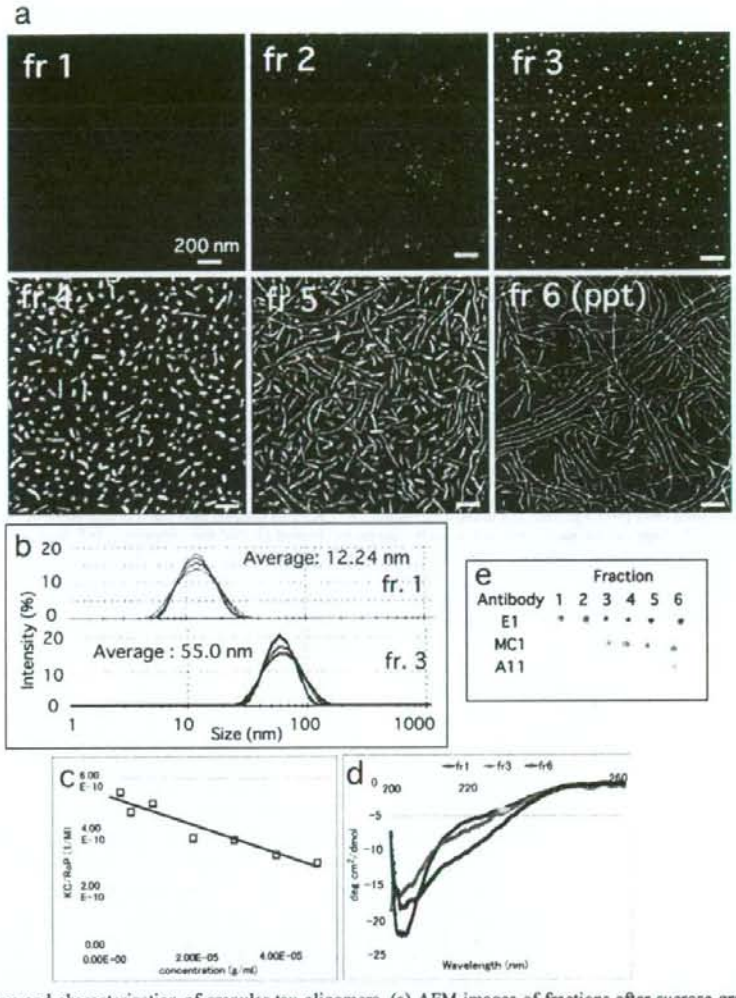

FIGURE 3: Purification and characterization of granular tau oligomers. (a) AFM images of fractions after sucrose gradient centrifugation. The scale bar is 200 nm. (b) Size distribution of soluble tau (fraction 1) and granular tau (fraction 3) as determined by dynamic laser light scattering. Fraction 1 displayed a distribution similar to that of monomeric tau species. Fraction 3, however, displayed a distribution of structures distinct from that of fraction 1, indicating that nonaggregated tau species do not contaminate fraction 3. (c) Analysis of the granular tau oligomer fraction using static laser light scattering. Debye plot of KC/RoP for different tau concentrations (□). The *y*-intercept value of the best linear fit indicates the approximate reciprocal of the molecular mass of granular oligomeric tau. (d) CD spectrum of fractions 1 (soluble tau oligomer), 3 (granular tau oligomer), and 6 (tau fibril). (e) The same amount of tau in each fraction was dotted onto nitrocellulose membranes and probed with the indicated antibodies.

(Figure 4a,b). These results strongly suggest that tau fibrils stem from granular tau oligomers or, in other words, that the granular tau oligomer is an intermediate form of tau fibril.

To confirm that granular tau aggregates form before the formation of tau fibrils in vivo, we purified, by immunoaffinity purification and sucrose gradient centrifugation, granular tau aggregates from human frontal cortex of cases evaluated to be at different Braak stages. As with the recombinant tau aggregation experiment, we detected granular tau oligomers in fraction 3 (Figure 4 of the Supporting Information) derived from Braak stage V samples (which have NFTs) (Figure 4e). Then, we could also detect them in fraction 3 derived from Braak stage 0 samples (which have no NFTs) (Figure 4e). The amount of granules in the Braak stage 0 samples, however, was significantly low. We also examined PHF-tau in Braak stage 0, I, III, and V samples by using a precipitation method (*14*) and found high levels of PHF-tau in Braak stage V brains but no detectable levels of PHF-tau in Braak stage 0, I, and III brains (*10*). These observations are consistent with the pathological evaluations of these brains.

Quantitative analysis showed increased levels of granular tau even in samples at Braak stage I, a stage characterized by the lack of NFTs in the frontal cortex. This finding suggests that tau granules accumulate far before tau fibrils form. Similar to what we found in our in vitro tau aggregation

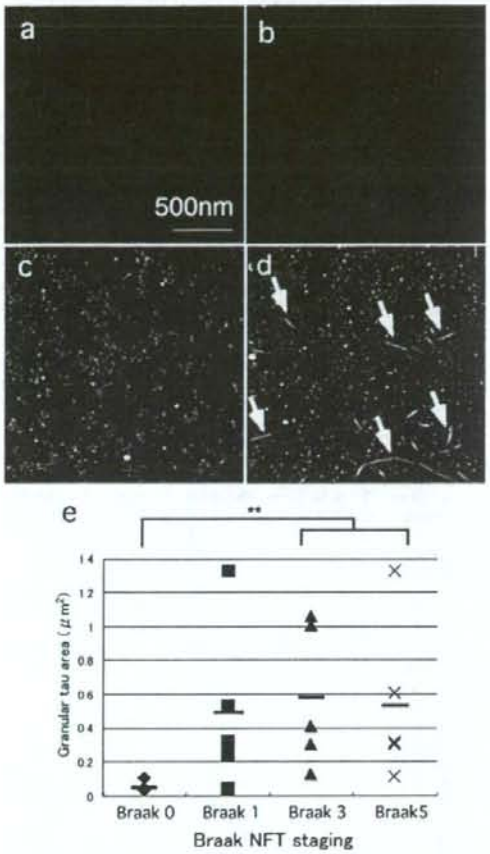

FIGURE 4: Tau filaments generated from granular tau oligomers. (a−d) AFM images of fractions 1 (a and b) and 3 (c and d), before (a and c) and after (b and d) the samples had been concentrated in the absence of heparin. Although concentrated fraction 1 had no structures, concentrated fraction 3 generated filaments (arrows). (e) The granular tau oligomer was purified as described in Materials and Methods from pathologically staged frontal cortex samples. Quantitative measurements of tau present in fraction 3 were derived from NIH-image 1.62 and are represented as the area (square micrometers) occupied by tau granules Two asterisks denote $p = 0.0155$ (Kruskal Wallis test).

experiments, high concentrations of granular tau oligomers in vivo may also lead to tau fibril formation in the brains of individuals with AD. Thus, granular tau oligomers may also represent an intermediate structure of tau during tau fibril formation in the human brain.

DISCUSSION

Tau Filaments Develop from Granular Tau Oligomers. Here we report that 40mer tau oligomers form granular structures having an MC1 epitope, indicating that this granular tau oligomer consists of conformationally changed tau. Partially folded tau monomers that are distinct from native tau monomers and that display a reduced level of random coiling but an increased level of β-sheet conformation have been reported previously (*15*). This type of conformation is similar to that displayed by granular tau oligomers; therefore, granular oligomers may be composed of these monomers.

Fibrils have a tendency to take on β-sheet conformations and also stain positively for anti-oligomer A11 antibody (*11*), which is consistent with our finding that A11 specifically recognizes proteins having either β-barrel or β-sandwich structures (Y. Yoshiike and A. Takashima, unpublished data). Therefore, tau fibrils may be composed of an assembly of granular tau aggregates having a β-sheet structure. Smaller granules of tau oligomers may grow by binding with soluble tau. Once the oligomer reaches a size of 20 nm, binding of granular tau oligomers enables tau fibrils to develop. This premise is consistent with our observation that only granular tau oligomers were detectable in the early stages of incubation, and the fact that fibrils appeared after longer incubations and CBB staining after electrophoresis in each fraction also support this idea (Figure 3 of the Supporting Information). After incubation for 7 months (5500 h), all tau monomers and granular tau oligomers had converted into filaments (data not shown). These observations are consistent with our hypothesis that the granular tau oligomer represents an intermediate form of tau filament.

In prions, complex pathways determine whether monomers derived from dissociated oligomers convert into filaments (*16*). Using our recombinant tau aggregation system, we examined fraction 3 to determine whether tau oligomers dissociate to form monomers, but we found no monomer contamination in fraction 3 (Figure 3b). After concentrating soluble tau and granular tau fractions (fractions 1 and 3, respectively), we found that granular tau, not soluble tau, is capable of forming filaments without additional heparin. This indicated that granular tau represents an intermediate form but that soluble tau does not. The mechanism underlying filament elongation by binding of granular tau oligomer needs further clarification.

Granular Tau Oligomers in Human Brain. Granular tau oligomers have been found in human brains. These oligomers consist of highly phosphorylated tau and are similar in size to granular tau oligomers derived from recombinant tau (*10*). PHFs could also be broken down into granular tau oligomers as well as filaments derived from recombinant protein (Figure 5a,b of the Supporting Information), further confirming the intermediary role of the granular tau oligomer during PHF formation in the human brain.

In the aged brain, PHF formation may occur when the level of granular tau oligomers increases. Although we found that non-AD brains contained no histologically verified NFTs, these brains did contain granular tau oligomers, albeit fewer than did AD brains. Interestingly, we also detected increased granular tau oligomer levels in brains showing early stage tau pathology. This was consistent with our immunochemical findings showing that granular tau oligomers are immunoreactive for MC1, which was recently reported to be a good indicator of early stage tau pathology in the frontal gyrus, even in the absence of NFTs (*17*). These biochemical data suggested that the formation of a granular tau oligomer precedes NFT formation. Moreover, we found significant differences in the number of granular tau oligomers in Braak stage 0 and I brains (*10*) but not in an oligomer-occupied area per field. We did find, however, significant differences